Detailed Measurements of a Diffusive Supersonic Wave in a Radiatively Heated Foam

C. A. Back, J. D. Bauer, O. L. Landen, R. E. Turner, B. F. Lasinski, J. H. Hammer, M. D. Rosen, L. J. Suter, and W. H. Hsing

Lawrence Livermore National Laboratory, L-21, P.O. Box 808, Livermore, California 94551

(Received 11 August 1999)

We have made the first detailed measurements of a diffusive supersonic radiation wave in the laboratory. A 10 mg/cm^3 SiO_2 foam is radiatively heated by the x-ray flux from a laser-irradiated hohlraum. The resulting radiation wave propagates axially through the optically thick foam and is measured via time-resolved x-ray imaging as it breaks out the far end. The data show that the radiation wave breaks out at the center prior to breaking out at the edges, indicating a significant curvature in the radiation front. This curvature is primarily due to energy loss into the walls surrounding the foam.

PACS numbers: 52.25.Nr, 52.50.Jm, 52.70.–m

Large laser facilities have enabled experimental investigations of phenomena associated with the radiative heating of matter. Marshak first considered one-dimensional radiative heating of a semi-infinite medium in a seminal paper [1]. Extensive analytic analysis is found in the classic text of Zel'dovich and Raizer [2] which discusses the relevant energy balance and radiation transport equations. In these references, the diffusive nature of supersonically radiatively heated material is characterized by a heat wave penetration speed that varies as the square root of time for a constant temperature source. More recently radiative heating has been observed in the laboratory by an ionization wave in an optically thin sample [3] or by thermal emission in an optically thick sample [4] modeled in an idealized planar geometry [5]. In the ionization wave experiments, the propagation length is limited to $\sim$1 mean free path and is often weakly supersonic or transonic which cannot be easily described by diffusion approximations. The optically thick clearly diffusive experiments are not fully supersonic.

In this Letter we describe the first observation of a supersonic radiation wave heating a sample that is a few optical depths in all directions. Furthermore, the effects of the finite transverse dimensions of the sample, which have not been discussed before, are clearly observed. These data provide clean signals of the propagation and shape of the radiation front. Both are significantly affected by the loss of energy to the structural support wall surrounding the test sample. Furthermore, the experimental spatial intensity profile is measured in enough detail to distinguish between different opacity models of the sample.

In the experiment we radiatively heat a 3 mm diam cylinder that is mounted on the side of a hohlraum radiative enclosure. The sample is a 10 ± 1 mg/cc SiO_2 foam of variable lengths and is shown schematically in Fig. 1. The face of the foam was parallel to the hohlraum axis and mounted at a radial distance of 1.7 mm. A 12 ns long laser square laser intensity pulse heats the hohlraum and creates an x-ray flux that increases in time. This intensity profile was obtained at the Omega Facility by using forty-eight 2 ns long 3ω beams, which are staggered in sets of eight every 2 ns for six contiguous time periods. The beams were pointed through 2.5 mm diam laser entrance holes (LEH) in the end caps of an 8 mm long, 4.8 mm diam cylindrical hohlraum. The x-ray drive temperature, T_r, peaks at approximately 85 eV at the end of the 12 ns pulse.

The SiO_2 foam sample was cast into a 25 μm thick Au ring that provided mechanical support. The outside face of the foam cylinder was masked by Mylar to form a 300 μm wide slit in order to define the area of foam viewed by the diagnostics. The samples were fabricated in 3 mm diam rings of four different lengths: 0.5, 1.0, 1.5, and 2.0 mm. The radiation wave propagates axially down the cylindrical foam and breaks out of the exterior face. Different lengths permit direct comparisons with simulations over a range of radiative propagation lengths. The diameter was chosen to provide a radiation wave that was as planar as practical, limited by the foam fragility, hohlraum size, and radiation drive.

A 2000 Å period Au transmission grating spectrometer coupled to an x-ray streak camera detects the foam emission. It viewed the exterior face and was oriented to spatially resolve the unmasked strip of foam in the long dimension with a resolution of 80 μm. Inside the diagnostic, a slit was positioned after the grating to select dispersed x rays with $h\nu = 250$ eV and a spectral bandwidth of $\sim$10 eV. A 5 μm parlylene-n filter reduced the grating

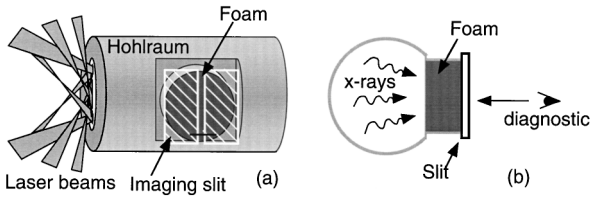

FIG. 1. Schematic of hohlraum with foam mounted on the side. The side view is shown in (a) with the laser beam illumination through the LEH. A cross-section view in (b) shows the radiation from the cavity heating the foam.

 0031-9007/00/84(2)/274(4)$15.00

response in second order to 2×10^{-3} of first order. The spectral energy band was centered at 250 eV to match the Rosseland mean photon energy at $\sim 4T_r$.

Other diagnostics included a set of x-ray diodes and a gated x-ray imager. The diodes were coupled to filters and x-ray mirrors to measure the radiation drive [6]. The imager provides two-dimensional spatial images of the radiation wave breakout. These images, recorded for $h\nu = 250$ eV, allowed corroboration of the timing and spatial intensity distribution of the radiation.

An example of the transmission grating data from the 1 mm long foam is shown in Fig. 2. Intensity traces along the temporal direction (horizontal) provide the breakout time of the heated sample, while intensity traces along the radial direction (vertical) provide information about the energy loss of the heat wave in a finite diameter geometry. Both aspects of the measurement are critical to understanding the radiation wave propagation. The data show that the radiation wave initially breaks out at the center of the foam and eventually breaks out at the edge ~ 2 ns later.

A simple scaling of the breakout time $t_{\rm bk}$ for a given foam length can be estimated by the internal energy divided by the product of the radiant flux, $\sim T_r^4$, times the mean free path. The SiO_2 opacity in the appropriate temperature range scales as T_r^3, while the internal energy goes as $T_r^{1.3}$. Hence, for a constant T_r, and assuming equilibrium ($T_r = T_e$),

$$t_{\rm bk} \propto T_r^{1.3} T_r^{-4} T_r^{-3} = T_r^{-5.7}.$$

This strong dependence on T_r makes it important to measure T_r to provide input to simulations that are used in comparisons with breakout data. This was measured on separate supplementary shots where the x-ray diode array had a line of sight onto an unirradiated portion of the hohlraum wall. The measured radiation drive is shown in Fig. 3 for this series of experiments. The measured temperature peaked at 85 eV $\pm$ 7%, giving an x-ray flux of 5.4×10^{12} W/cm^2. Hohlraum drive measurements have been studied in scaled geometries [7] and extensive modeling of this hohlraum drive will be presented in a longer paper. Figure 3 does show that T_r is not constant, but rises slowly with time as expected for hohlraums driven by nearly constant laser fluxes [8]. For this pulse it scales as $T_0(t/t_0)^{0.28}$ where t is time after the start of the laser pulse and T_0 is the temperature at a finite time t_0. Thus for the radiation flux in these experiments the breakout time scales more correctly as $T_0^{-2.2}$.

Intensity lineouts in time provide the position of the radiation wave as a function of time for four lengths. The breakout times at the center are 3.8, 6.7, and 11.1 ns for the 0.5, 1.0, and 1.5 mm long foams, respectively, and the intensity lineouts are shown in Fig. 3 along with those calculated by the simulations using the measured T_r. No breakout signal was detected within the 18 ns temporal window of the instrument for the 2 mm long foam. The breakout times are measured to high accuracy because of timing fiducials recorded simultaneously on the film. The timing errors are 3%, 3%, and 5% for the 0.5, 1.0, and 1.5 mm long foams, respectively.

The instrument initially views through cold foam, therefore the rise time of the emission is expected to be the time it takes the Marshak wave to propagate through approximately 1 mean free path (MFP) of cold material. The thermal wave in a form at $T_r = 60$ eV propagates at a velocity of 160 μm/ns. Since the cold MFP at 250 eV is 40 μm, this gives a rise time of ~ 300 ps which is in agreement with data. As the foam heats up, the emission at these photon energies is dominated by line emission, which remains at fairly high opacity and does not vary significantly. Over the relevant foam temperature range of 40–60 eV, the MFP at 250 eV predicted by the OPAL code [9] has risen to only 50–100 μm. This is significantly shorter than the Rosseland MFP (~ 550 μm) which determines the axial temperature gradient scale lengths. Hence, this shallow and temperature-insensitive MFP at 250 eV allows an accurate measure of the radial variation (i.e., at fixed axial distance) in the foam temperature after breakout of the radiation wave.

Simulations using OPAL opacity data were performed using the measured T_r. For the 0.5 and 1.0 mm long foams,

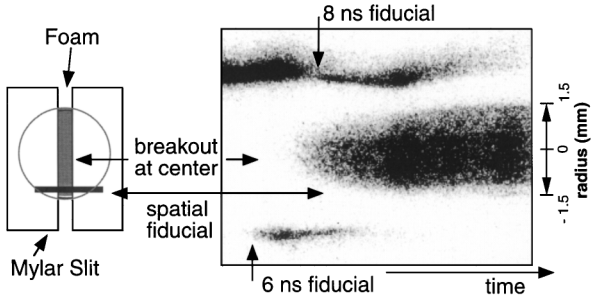

FIG. 2. Diagnostic view of foam sample and example of data. The foam emission is spatially imaged in the vertical direction and integrated over the slit width. On the data, emission appears black and the horizontal axis represents time. Timing fiducials are x-ray signals created by laser beams irradiating the outside of the hohlraum body.

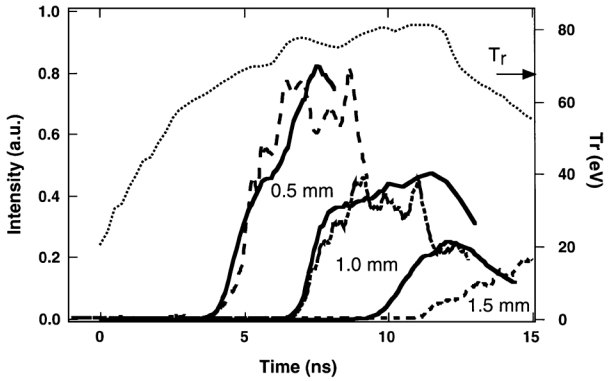

FIG. 3. Intensity vs time lineouts at foam center for three different length foams. Dashed lines show data; solid lines show calculations. The measured radiation drive temperature is plotted along the right-hand axis.

they are early by ~0.3 ns. For the longest foam, calculations are ~1.5 ns earlier. Based on intensity levels of the signal predicted by the simulations, the emission from the 2.0 mm long foams was probably below the detection level of the diagnostic. In these foams the Mach number of the radiation wave at the average foam temperature of 60 eV is ~2.5 (the sound speed is ~60 μm/ns); therefore the radiation wave heats the material before significant hydrodynamic motion occurs.

The simulations of these experiments require accurate calculations of the opacity of the material, the internal energy, the hydrodynamics, and the radiation temperature. The opacity and internal energy are well modeled with OPAL for mid-Z elements [10]. Simpler average atom opacity models produce breakout times roughly 15% later. The hydrodynamics of Au hohlraum environments have been studied in inertial confinement fusion targets that operate in very similar plasma regimes, and no significant hohlraum plasma dynamics are expected to play a role in the sample heating during the time frame of these measurements.

Simulations with a frequency dependent source are found to affect the calculation by ~5%, so breakout times are not significantly affected by details of the frequency distribution. The breakout times predicted by the codes have ~15% error, based on the error on the measurements and the above T_r sensitivity analysis. Therefore agreements between the data and simulations are reasonable and further analysis of late time discrepancies will require better T_r measurements.

Near the edges, the delayed breakout indicates that the radiation wave is no longer planar. The compound effects of the drive uniformity and foam-support interface are best understood by considering the spatial intensity traces along the radial direction. At any point in time, the emission is clearly lower in intensity at the edges. An example of a radial lineout taken from the 1 mm long foam data in Fig. 2 is shown in Fig. 4. The data, shown by squares, is taken at 9.5 ns, which are 2.5 ns after the initial breakout. The radiative hydrodynamic calculations using a detailed or an average atom opacity model are also shown in the figure. Data that are taken independently on the gated x-ray imager, which obtains a two-dimensional image in an 80 ps temporal snapshot, confirm the intensity distribution shown in Fig. 4. The radially varying intensity distribution could be the result of three factors: the radially dependent solid angle subtended by the source, possible obscuration of the source by the expanding Au support wall as it is heated, and the energy loss to the walls.

The first factor which may produce a curved intensity lineout is the reduced solid angle of the x-ray source (commonly known as the viewfactor) subtended by a point at the radial edge relative to the solid angle subtended by a point at the foam center. The shadowing of the foam side walls will reduce the flux at the edges. Viewfactor calculations show that this radial effect is less than 5% at 1.3 mm from the center. If we compare the flux at 1 axial optical depth into the foam and 1 mm radially from the center,

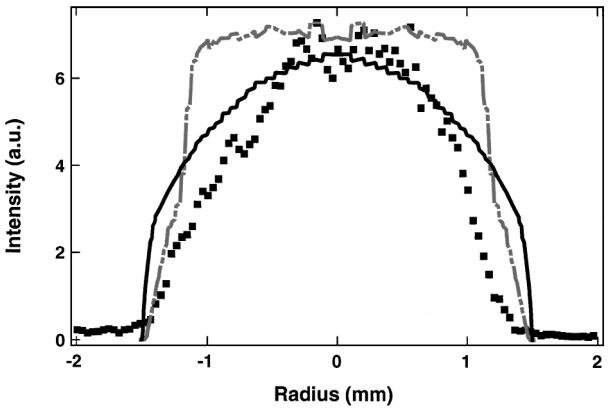

FIG. 4. An example of radial lineouts at 9.5 ns after the x-ray drive starts. The squares are the data, the solid line is the calculation using the OPAL model for the SiO_2, and the dotted line is the calculation using an average atom model.

the viewfactor is negligibly reduced, but the measured radial lineout has dropped 38% relative to the center. At longer lengths, $\tau > 1$, the viewfactor is more nearly constant across the face. In addition, as the Au wall in the actual target heats up, it reradiates energy, further mitigating the reduced edge viewfactor. Although the viewfactor is a contributor, it does not account for the measured radial intensity drop.

A second possible contribution to the curvature is the reduction of the viewfactor due to heating and expansion of the Au support which would reduce the effective diameter of the foam tube. At the time of the measurement shown in Fig. 4, simulations show that the Au wall at the source entrance expands inward about 200 μm from the 1.5 mm edge, and this may obscure the incident flux. When represented by a smaller effective entrance aperture of 2.6 mm, the drop in flux 1 mm from the center is predicted to be only 13% by the viewfactor analysis, which is still significantly less than the 38% measured. Hence a reduced edge viewfactor, with or without wall closure, does not sufficiently account for the radial variation in flux or breakout time.

The third cause for the radial variation is that energy goes into heating the Au support ring and leads to a decreasing temperature from the center to the radial edge. Because the edge is ~3 mean free paths from the center, the edge effects do not immediately affect the radiation propagation at the center. However, due to the continued energy loss to the walls, the resulting temperature gradient will always produce a curved radiation wave breakout because the T_r-dependent velocity of the radiation wave is lower at the edges.

A simple analytic model for the energy balance in this target gives some qualitative insight. If we assume that a simple foam cylinder in an Au tube is heated from one side by a constant flux, we can calculate the total energies of heating due to the propagation of a planar diffusive wave using scalings of the SiO_2 and Au internal energy and opacity with T_r. An upper bound on the loss

of energy due to heating Au compared to the total energy heating the foam plus Au is 15%, 28%, and 38% at the three lengths that break out during the x-ray drive. (Recall that the fourth length was not observed to break out.) The fraction of energy heating the wall for longer foams increases because the ratio of wall area to unheated foam area increases with longer foam lengths. When the energy lost into heating the wall is larger than the energy heating the foam sample, the radiation wave can no longer propagate down the foam. At the 1.5 mm length, a significant amount of energy is expended heating the wall according to the simple model. Detailed radiative hydrodynamic simulations yield 7%, 14%, and 22%, also indicating that a nontrivial part of the energy loss is due to heating the Au. These percentages are lower and more realistic because the simple model does not self-consistently account for transverse temperature gradients in the foam and thus overestimates the energy into the wall. Hence, this third factor, the energy loss, is the primary cause of the curvature in the breakout timing or the spatial intensity lineouts.

To further characterize the radiative heating, we also infer the number of mean free paths in the heated foam. At 250 eV the cold foam radius is 38 MFP across, with a range from 13–50 MFPs in the axial direction for the shortest to the longest foam. According to simulations, at breakout the foam attains a mass-weighted average temperature of 60 eV which yields an integrated Rosseland MFP of $\sim$2.5 through the axis length of the 1.5 mm long foam, the longest foam where the breakout was observed. To deduce the radial number of mean free paths, we normalize the intensity at the center, assuming a center temperature of 60 eV, as given by the calculations. The measured drop in the typical intensity profile then implies a temperature of $\sim$45 eV at the edge. Based on the measured radial variation in emission, the radial optical depth, τ, measured at a given time is

$$\tau(r) = \int_0^\infty \kappa(r')\rho \, dr' = \int_0^\infty \frac{3.74}{T_r(r')^3} \, dr',$$

where r is in cm and T_r is in eV. We have used a T_r^{-3} opacity scaling for SiO_2 over this range of temperatures and a constant density of 10 mg/cc. In the case of the intensity lineout shown in Fig. 4, this gives an optical depth of $\sim$3.5 in the radial direction. If we had assumed the foam was uniformly 60 eV, this would be $\sim$3 MFP. The value we measure is higher because the foam temperature is lower at the edge, and the MFP is not constant, dropping from $\sim$550 to 230 μm with the temperature change.

The simulations using the detailed OPAL opacity model clearly fit the radial intensity data more closely than those using an average atom model, as shown in Fig. 4. Although it is the Rosseland mean which determines the radiation heat wave propagation, the emission we measure is dominated by the opacity at the detected photon energy, $h\nu = 250$ eV, which may be more highly dependent on the opacity model. At this energy, the $n = 2$–3 transitions in oxygen and silicon dominate and an average atom model is inadequate. A comparison of the frequency-dependent opacity of two models shows differences up to an order of a magnitude in the opacity at $h\nu = 250$ eV as the temperature in the radiation front varies between 40 to 80 eV. This produces drastically different predicted radially resolved emission patterns. By contrast, the Rosseland mean opacity is virtually the same for the two opacity models at 60 eV, and 60% higher than the average atom opacity at 40 eV. The choice of the opacity model affects the breakout times by only $\sim$15% because they depend on mean values, i.e., the Rosseland mean opacity averaged over a rising temperature profile. The radial intensity profile, however, is dependent on the opacity model at a particular photon energy and hence can be radically affected.

This paper conclusively shows supersonic propagation greater than one mean free path. Furthermore, significant curvature in the radiation front profile is observed in samples that are many mean free paths in diameter, and we show that this curvature is primarily caused by the energy loss to the walls. Thus, the shape of the radiation wave, as witnessed by the breakout, is dependent on a combination of the foam and wall material properties. In particular, we are able to make new detailed measurements which can be fit only by advanced opacity models. These experiments provide data which serve as a basis for future radiation transport experiments in finite geometry.

The authors thank the LLNL target fabrication crew, Dr. J. Soures, S. Loucks, and the Omega laser crew at the Laboratory for Laser Energetics. This work was performed under the auspices of the U.S. Department of Energy by the Lawrence Livermore National Laboratory under Contract No. W-7405-ENG-48.

[1] R. E. Marshak, Phys. Fluids **1**, 24 (1958).
[2] Y. B. Zel'dovich and Y. P. Raizer, *Physics of Shock Waves and High Temperature Hydrodynamic Phenomena* (Academic, New York, 1966).
[3] T. Afshar-rad *et al.*, Phys. Rev. Lett. **73**, 74 (1990); D. Hoarty, A. Iwase, C. Meyer, J. Edwards, and O. Willi, Phys. Rev. Lett. **78**, 3322 (1997); D. Hoarty *et al.*, Phys. Plasmas **6**, 2171 (1999).
[4] J. Massen *et al.*, Phys. Rev. E **50**, 5130 (1994); J. C. Bozier, G. Thiell, J. P. Le Breton, S. Azra, M. Decroisette, and D. Schirmann, Phys. Rev. Lett. **57**, 1304 (1986); R. Sigel *et al.*, Phys. Rev. Lett. **65**, 587 (1990).
[5] R. Sigel, K. Eidmann, F. Lavarenne, and R. F. Schmalz, Phys. Fluids B **2**, 199 (1990); K. Eidmann, R. F. Schmalz, and R. Sigel, Phys. Fluids B **2**, 208 (1990).
[6] H. N. Kornblum, R. L. Kauffman, and J. A. Smith, Rev. Sci. Instrum. **57**, 2179 (1986).
[7] R. L. Kauffman *et al.*, Phys. Rev. Lett. **73**, 2320 (1994).
[8] M. D. Rosen, Phys. Plasmas **3**, 1803 (1996).
[9] F. J. Rogers, C. A. Iglesias, and B. G. Wilson, Astrophys. J. **397**, 717 (1992).
[10] T. S. Perry *et al.*, Phys. Rev. Lett. **67**, 3784 (1991); J. M. Foster *et al.*, Phys. Rev. Lett. **67**, 3255 (1991).